

# Identification of Emotionally Stressful Periods Through Tracking Changes in Statistical Features of mHealth Data

Younghoon Kim<sup>1</sup>, Sumanta Basu<sup>1</sup>, and Samprit Banerjee<sup>†2</sup>

<sup>1</sup>Cornell University

<sup>2</sup>Weill Cornell Medicine

November 11, 2025

## Abstract

Identifying the onset of emotional stress in older patients with mood disorders and chronic pain is crucial in mental health studies. To this end, studying the associations between passively sensed variables that measure human behaviors and self-reported stress levels collected from mobile devices is emerging. Existing algorithms rely on conventional change point detection (CPD) methods due to the nonstationary nature of the data. They also require explicit modeling of the associations between variables and output only discrete time points, which can lead to misinterpretation of stress onset timings. This is problematic when distributional shifts are complex, dependencies between variables are difficult to capture, and changes occur asynchronously across series with weak signals. In this study, we propose an algorithm that detects hotspots, defined as collections of time intervals during which statistical features of passive sensing variables and stress indicators shift, highlighting periods that require investigation. We first extend the moving sum (MOSUM) scheme to detect simultaneous changes both within and across series, and then define hotspots in two ways: using distance-based test statistics and confidence intervals. The proposed method tracks local changes in combined distributional features, enabling it to capture all types of simultaneous and asynchronous change. It does not require a specific functional relationship between series, and the results are expressed as intervals rather than as individual time points. We conduct simulations under varying signal strengths with mixed and asynchronous distributional shifts, where the proposed method outperforms benchmarks. Results on hotspot identification indicate that the two definitions are complementary. We further apply our method to ALACRITY Phase I data, analyzing hotspots from patients' stress levels and activity measures.

Keyword: Change point detection, moving sum, ensemble, bootstrap, mHealth, mental health

## 1 Introduction

Emotional stress is the mental and physiological strain that occurs when individuals perceive that demands exceed their coping resources. In older adults, it often leads to mood disturbances and reduces the effectiveness of psychotherapy (e.g., Doraiswamy et al., 2002, Murphy et al., 2016).

---

<sup>†</sup>Corresponding author. Email: sab2028@med.cornell.edu

In particular, older patients with mood disorders are more likely to experience reduced quality of life, suicidal behaviors, and elevated all-cause mortality. In this context, identifying individuals' stress status is crucial. With the development of mobile health (mHealth) technologies, collecting real-time data has become easier, enabling more timely monitoring of emotional stress (e.g., Lee et al., 2021, Solomonov et al., 2025). Patients themselves can report their stress levels and related feelings through mobile devices such as smartphones and wearables, and their emotional status in daily life can be tracked without the need for in-person visits to clinical experts. Automatically detecting the onset of emotional stress could also enable timely interventions, allowing clinicians to respond proactively and potentially prevent a marked decline in mood or health.

Passive sensing variables are datasets collected by mHealth devices through sensors without requiring active input from the user. These variables often capture physiological signals, such as skin temperature, heart rate variability, and blood pressure, which can reflect changes in stress levels (e.g., Maharjan et al., 2021, Sheikh et al., 2021). In addition to physiological measures, behavioral indicators can also serve as passive sensing variables. Patterns of physical activity, including body movement, time spent in social activity, and sleep quality, provide complementary information about a person's stress state. Behavioral measures are easy to track with widely available commercial devices, do not require research-grade equipment, and can be collected naturally in daily life. By using these passive sensing variables, it is possible to monitor changes in stress levels in real time, enabling timely identification and intervention (e.g., Sano et al., 2018, Saylam and İncel, 2023).

The goal of studying passive sensing variables in this context is thus to uncover their associations with stress, which can later be used for prediction through machine learning (ML) algorithms when self-reported emotional feelings are unavailable. However, it is quite common that directly applying conventional ML methods to these datasets often leads to poor performance (e.g., Vos et al., 2023, Bustamante et al., 2024, Del Angel et al., 2025). It is because both passive sensing variables and stress levels are typically non-stationary; Their mean and variability may change across different time periods, and these local variations can become obscured when analyzed over the entire observations.

To address this challenge, change point detection (CPD; e.g., Aminikhanghahi and Cook, 2017, Truong et al., 2020, Cho and Kirch, 2024, for comprehensive surveys) can be applied as a preprocessing step to identify time points where data characteristics shift, allowing each segment to be analyzed or labeled separately before being used in ML models. In the context of stress detection from passive sensing variables, pre-defined rule-based methods were widely accepted (e.g., Kyriakou et al., 2019, Moser et al., 2023). Recently, CPD algorithms have emerged as a data-driven alternative for identifying transitions in stress levels. For example, Hosseini et al. (2022) applied a CPD algorithm (Truong et al., 2018) to their multimodal sensor data to identify moments of abrupt physiological or behavioral change that corresponded to transitions between low- and high-stress states in nurses during their work shifts. For the stress detection of older patients, Kim et al. (2025) proposed a framework that combines the CPD algorithm by Matteson and James (2014) with a linear model linking passive sensing variables to stress levels. Their findings demonstrated that CPD can detect meaningful changes in stress patterns and that accounting for distributional shifts in the data improves the prediction of future stress states.

However, existing algorithms still rely heavily on off-the-shelf CPD methods and often require specific modeling assumptions, such as linear or even nonlinear relationships between passive sensing variables and stress levels. These methods may fail when discrepancies arise between the detected change points in passive sensing variables and stress levels, or between the estimated timings

and those identified through visual inspection. Furthermore, missing the exact or even nearby onset times of stress-level changes can undermine the reliability of passive sensing variables. Such limitations pose challenges for clinical researchers seeking to validate their effectiveness as digital biomarkers in future studies (e.g., Mohr et al., 2017, Gomes et al., 2023).

### 1.1 Motivative Examples

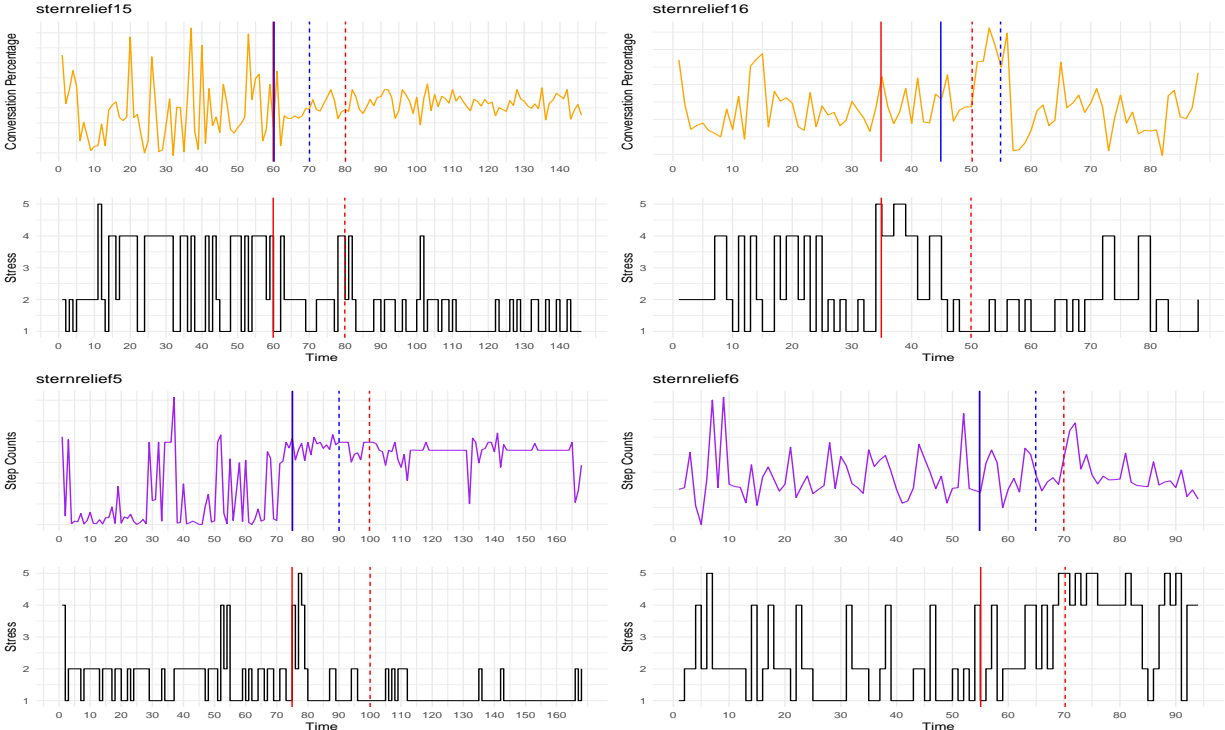


Figure 1: Representative patterns in passive sensing variables and stress levels from four patients in ALACRITY Phase I data. In each panel, the colored lines represent passive sensing variables, and the black lines represent stress levels. The red solid and dashed lines indicate the expected start and end points of changes in stress levels, while the blue solid and dashed lines indicate the expected start and end points of changes in the passive sensing variables.

Examples of pairs of passive sensing variables and stress levels from four different patients are shown in Figure 1. The details of the series are given in Section 5.3. The distributional shifts in each of the two series are likely located between the solid and dashed lines, as indicated by visual inspection. However, although the intervals in which these changes occur overlap within each patient’s case, they are asynchronous (i.e., they do not occur at the same time). Moreover, for passive sensing variables, the types of changes in each series cannot be clearly categorized into a single type, such as changes solely in means or variances.

The limitations of conventional CPD algorithms can be summarized as follows. First, traditional CPD methods typically detect only a single type of distributional change. However, as shown in Figure 1, passive sensing variables and stress levels often exhibit simultaneous changes in both mean and variance. This highlights the need for a more flexible framework capable of identifying local changes across multiple statistical characteristics occurring at the same time. Second, conventional

CPD algorithms usually report specific change points, assuming that changes occur instantaneously and then persist. This assumption is unlikely to hold for our data, where changes may occur gradually or at any point within the given intervals, as illustrated by the solid and dashed bands. Moreover, in paired series, the timing of distributional changes may not coincide, suggesting that results should be represented as intervals rather than discrete points. Third, overlapping intervals where change points are likely to occur indicate potential associations between passive sensing variables and stress levels. However, given the observed patterns, such relationships cannot be adequately captured by models assuming a fixed functional form. Finally, as shown in Figure 1, the low strength of signals in both series further complicates the detection of change points.

## 1.2 Contributions

In this article, we develop an algorithm that tracks simultaneous and potentially asynchronous changes in low-level statistical features, focusing on changes in the mean and variance of passive sensing data and stress levels. These features are easy to interpret and play an important role in prediction. The algorithm serves as a tool for clinical experts to investigate associations between stress and human behavior by monitoring changes in these time series.

This study makes several novel contributions. First, it introduces the concept of hotspots and proposes a data-driven method to identify them. This addresses a key limitation of conventional CPD algorithms, which typically detect only isolated time points rather than extended periods of change. By tracking local variations in statistical features, the algorithm can detect more candidate time points corresponding to actual, though possibly subtle, shifts in stress levels. Second, it jointly tracks changes across multiple distributional features, capturing diverse types of concurrent changes in a given series. This ensemble approach provides a more complete characterization of underlying dynamics than univariate metrics alone. Finally, the method is model-free: it does not assume a specific functional relationship between passive sensing variables and stress levels, while still accounting for their interdependent dynamics. The dependence structure is included as an auxiliary component, supporting detection of both within-series and cross-series changes in means and variances.

## 1.3 Organization of Paper

The remainder of this article is organized as follows. Section 3 briefly describes the definition of hotspots. Section 3 focuses on detecting change points for various types of changes. This involves the modification of the existing CPD algorithm applied in our proposed method. Section 4 describes how initially identified change points are aggregated using ensemble strategies to generate robust change regions. The numerical experiments evaluating the performance of the method are presented in Section 5. Finally, Section 6 concludes with a discussion.

## 2 Definition of Hotspots

Hotspots are defined as collections of time intervals during which clinical experts are advised to pay attention to changes in features derived from passive sensing variables. These features capture aspects of human behavior (e.g., mobilization, sociability, and sleep), and changes in these behaviors around specific time points may be strongly associated with variations in stress levels. The intervals

are characterized by distributional shifts in both passive sensing data and stress levels, under the assumption that variations in one series may influence or be influenced by variations in the other.

The proposed algorithm proceeds in two main steps. First, it identifies specific time points at which changes are likely to occur, capturing different types of changes in the series. Second, for each type of detected change, it constructs neighborhood intervals around these points and combines them to form an ensemble of change regions. Consequently, the proposed method offers a flexible framework for identifying periods of behavioral and stress-related changes that are likely to be clinically meaningful.

### 3 Finding Change Points

As the first step of identifying hotspots, we find the change points where all different types of distributional shifts occur in either univariate or bivariate series.

Throughout the rest of the article, we denote a univariate passive sensing variable by  $X_t$  and stress levels by  $Y_t$ , where  $\{X_t\}$  and  $\{Y_t\}$  refer to subsets or complete sets of samples of  $X_t$  and  $Y_t$ , respectively.

#### 3.1 Preparations

To apply the proposed algorithm to the raw dataset, two preprocessing steps are necessary. First, we handle the discrete nature of the stress-level series by transforming them into continuous representations, enabling the use of statistical models and change point detection methods that assume continuous inputs. Second, we debias the passive sensing variables obtained from mobile devices to reduce the impact of recording errors and missing data.

In many cases, the stress-level series  $\{Y_t\}$  is not continuous but instead takes discrete values following a categorical distribution, such as a 5-point Likert scale (see second or fourth row in Figure 1). To facilitate statistical modeling and analysis that assume continuity, it is often useful to transform such discrete-valued data into a continuous form. Inspired by the treatment of quantile residuals (e.g., Dunn and Smyth, 1996), we apply a smoothed and randomized inverse cumulative distribution function (CDF) transformation. Specifically, for each observation  $Y_t$ , we define

$$\begin{aligned} U_t &:= \hat{F}_t(Y_t^-) + W_t \hat{\mathbb{P}}(Y_t = y), \quad y = 1, \dots, 5, \\ Z_t &:= \Phi^{-1}(U_t) \end{aligned} \tag{1}$$

where  $\hat{F}_t(\cdot)$  denotes the estimated CDF of the observed discrete-valued series  $\{Y_t\}_{t=1}^n$ ,  $W_t \sim \text{Unif}(0, 1)$  are independent random variables drawn at each time point, and  $\Phi^{-1}(\cdot)$  represents the inverse CDF of the standard normal distribution. This transformation effectively maps the discrete categorical responses into continuous latent variables while preserving their probabilistic structure (see the top panels of Figures 2 and Figures 3 below for the examples of the transformation (1)). In what follows, we regard  $\{Y_t\}$  as a continuous-valued data stream throughout the rest of this paper.

More importantly, raw passive sensing mHealth data often exhibit a downward bias due to device non-use (e.g., when the phone is turned off, not carried, or the app is inactive). The 2SpamH algorithm (Zhang et al., 2024) is a two-stage unsupervised preprocessing method developed to mitigate this bias in passively collected mHealth data. In the first stage, the algorithm evaluates the reliability of each observation using auxiliary indicators such as screen unlock counts, battery

variance, and app usage, allowing it to distinguish periods of true low activity from those resulting from device non-use. In the second stage, it applies bias-correction models to the subset of reliable data, ensuring that the retained measurements more accurately capture the user’s actual behavior. Further details of the algorithm are provided in Zhang et al. (2024). This preprocessing has already been applied to the real data used in Section 5.3.

### 3.2 Finding Simultaneous Change Points in Univariate Series

The moving sum (MOSUM; e.g., Bauer and Hackl, 1980, Chu et al., 1995, Hušková, 1990) is a widely used CPD procedure based on scan statistics (e.g., Abolhassani and Prates, 2021); by sliding the window across the series, the procedure quantifies the difference between the statistics computed from the observations before and after the window center to evaluate shifts in mean levels. Despite its simplicity, it has received less attention compared to global search methods using dynamic programming (e.g., Jackson et al., 2005, Killick et al., 2012) or other rolling-window-based estimators, such as binary segmentation (e.g., Vostrikova, 1981, Fryzlewicz, 2014). With further developments in scan-statistics-based CPD algorithms (e.g., Chen and Zhang, 2015) and the establishment of statistical properties of the MOSUM procedure Eichinger and Kirch (2018), it has regained attention. More recently, extensions of the MOSUM approach have been proposed to detect changes in variance (Messer et al., 2018), as well as the joint detection of mean and variance changes, referred to as Joint-MOSUM (Meier et al., 2021, Levajković and Messer, 2023), to detect changes in both the mean and variance of individual series.

Specifically, suppose the series  $\{X_t\}_{t=1}^n$  is given. The Joint-MOSUM algorithm identifies the specific time points at which changes are likely to occur. Let  $\mu_X(t_1, t_2)$  and  $\sigma_X^2(t_1, t_2)$  denote the population mean and variance (features) of  $\{X_{t_1}, \dots, X_{t_2}\}$  within time points  $t_1$  and  $t_2$  and their sample analogues

$$\bar{X}(t_1, t_2) = \frac{1}{t_2 - t_1 + 1} \sum_{t=t_1}^{t_2} X_t, \quad S_X^2(t_1, t_2) = \frac{1}{t_2 - t_1 + 1} \sum_{t=t_1}^{t_2} (X_t - \bar{X}(t_1, t_2))^2.$$

In this setting, the CPD algorithm is equivalent to performing a combined hypothesis test sequentially; For each time  $t = k$ , we test one of the following two hypotheses:

$$H_0(k) : \mu_X(k - G, k) = \mu_X(k + 1, k + G), \quad \sigma_X^2(k - G, k) = \sigma_X^2(k + 1, k + G), \quad (2)$$

with the corresponding alternative hypotheses  $H_A(k)$  defined as the negation of  $H_0(k)$ , indicating that either or both of the features have changed locally at time  $t = k$ . For notational simplicity, we will suppress  $G$  in these features and their sample analogs hereafter. The same hypothesis test is performed when  $\{Y_t\}_{t=1}^n$  is given.

Following the conventional MOSUM procedure, we first consider the difference in the local mean of  $X_t$  around the time point  $t = k$ ,  $k = 1, \dots, n$ , defined as

$$d\bar{X}(k) = \begin{cases} C_1 \sum_{t=1}^k (\bar{X}(1, 2G) - X_t), & k = 1, \dots, G - 1, \\ \bar{X}(k + 1, k + G) - \bar{X}(k - G + 1, k), & k = G, \dots, n - G, \\ C_n \sum_{t=n-G+1}^n (\bar{X}(n - 2G + 1, n) - X_t), & k = n - G + 1, \dots, n, \end{cases} \quad (3)$$

where  $C_1 = \frac{2}{\sqrt{k(2G-k)}}$  and  $C_n = \frac{2}{\sqrt{(n+1-k)(k-n+2G)}}$ . Using this, we define the rolling window estimator (detector) for the local change in the mean of  $X_t$  around  $t = k$  by

$$T_X^{(1)}(k) = \frac{d\bar{X}(k)}{S_X(k)}, \quad (4)$$

where  $\bar{S}_X^2(a, b)$  is the locally averaged variance of  $X_t$  at  $t = k$ , given by

$$\bar{S}_X^2(k) = \begin{cases} S_X^2(1, 2G), & k = 1, \dots, G-1, \\ \frac{1}{2}(S_X^2(k+1, k+G) + S_X^2(k-G+1, k)), & k = G, \dots, n-G, \\ S_X^2(n-2G+1, 2n), & k = n-G+1, \dots, n. \end{cases} \quad (5)$$

The rolling window estimator for local changes in the mean of  $\{Y_t\}$  around  $t = k$ , denoted by  $T_Y^{(1)}(k) = d\bar{Y}(k)/\bar{S}_Y(k)$ , is defined analogously.

The studies by Messer et al. (2018), Messer (2022) and Levajković and Messer (2023) have shown that this construction can also be applied to detect changes in variance. Specifically, the difference in the local variance of  $X_t$  around the time point  $t = k$ ,  $k = 1, \dots, n$ , is defined as

$$dS_X^2(k) = \begin{cases} C_1 \sum_{t=1}^k (S_X^2(1, 2G) - (X_t - \bar{X}(1, 2G))^2) & k = 1, \dots, G-1, \\ S_X^2(k+1, k+G) - S_X^2(k-G+1, k) & k = G, \dots, n-G, \\ C_n \sum_{t=n-G+1}^n (S_X^2(n-2G+1, n) - (X_t - \bar{X}(n-2G+1, n))^2) & k = n-G+1, \dots, n, \end{cases}$$

using the same constants  $C_1$  and  $C_n$  defined in (3). The rolling window estimator for the local change in the variance of  $\{X_t\}$  around  $t = k$  is then defined as

$$T_X^{(2)}(k) = \frac{dS_X^2(k)}{\bar{V}_X(k)}, \quad (6)$$

where  $\bar{V}_X^2(a, b)$  is the locally averaged kurtosis of  $X_t$  at  $t = k$ , given by

$$\bar{V}_X^2(k) = \begin{cases} V_X^2(1, 2G), & k = 1, \dots, G-1, \\ \frac{1}{2}(V_X^2(k+1, k+G) + V_X^2(k-G+1, k)), & k = G, \dots, n-G, \\ V_X^2(n-2G+1, n), & k = n-G+1, \dots, n, \end{cases} \quad (7)$$

where  $V_X^2(a, b) = \frac{1}{b-a+1} \sum_{t=a}^b ((X_t - \bar{X}(a, b))^2 - S_X^2(a, b))^2$ , using the locally averaged mean and variance defined in (5). The rolling window estimator for local changes in the variance of  $\{Y_t\}$  around  $t = k$ , denoted by  $T_Y^{(2)}(k) = dS_Y^2(k)/\bar{V}_Y(k)$  is defined similarly.

To test the hypothesis (2), by following Messer (2022) and Levajković and Messer (2023), we combine those detectors (4) and (6). The joint detector at time point  $t = k$  is defined as

$$J_X(k) = \begin{pmatrix} T_X^{(1)}(k) \\ T_X^{(2)}(k) \end{pmatrix} \in \mathbb{R}^2.$$

In addition, consider the covariance matrix as

$$\Gamma_X = \begin{pmatrix} 1 & \rho_X \\ \rho_X & 1 \end{pmatrix},$$

where

$$\rho_X := \frac{\mathbb{E}[(X - \mu_X)^3]}{\sqrt{\text{Var}(X - \mu_X)}\sqrt{\text{Var}((X - \mu_X)^2)}} := \frac{\kappa_X}{\sigma_X \nu_X}.$$

Its local sample analog around the time point  $t = k$ , denoted by  $\hat{\Gamma}_X(k)$ , is obtained by replacing  $\rho_X$  with  $\hat{\rho}_X(k)$ , where

$$\hat{\rho}_X(k) = \frac{\bar{\kappa}_X^2(k)}{S_X(k)\bar{V}_X(k)}, \quad (8)$$

with  $\bar{K}_X(k) = \frac{1}{2}(K_X(k+1, k+G) + K_X(k-G+1, k))$ , where

$$K_X(a, b) = \frac{1}{b-a+1} \sum_{t=a}^b (X_t - \bar{X}(a, b))^3.$$

The covariance matrix  $\hat{\Gamma}(k)$ , computed using the locally averaged skewness scaled by the locally averaged covariance and kurtosis (8), captures the association between local changes in mean and variance while circumventing the need to specify an explicit model for the dependence structure. Then we compute the Mahalanobis distance, used to detect the combined local changes at time point  $t = k$ , by

$$D_X^2(k) = J_X(k)' \hat{\Gamma}_X(k)^{-1} J_X(k). \quad (9)$$

Hence, we use the distance (9) as the test statistic at each  $t = k$ ,  $k = 1, \dots, n$ .

The Joint-MOSUM procedure identifies initial change points where the corresponding detectors (9) exceed the threshold determined by  $n$ ,  $G$ , and  $\alpha$ . However, no closed-form expression of the threshold exists (e.g., see Section 5 in Messer, 2022). Instead, we use the Monte Carlo simulation to compute the threshold. Specifically, for each  $b^{\text{th}}$  replication,  $b = 1, \dots, B$ , the threshold is computed as

$$D_n(G, \alpha)^{(b)} = \max_{G \in \mathcal{G}} \max_h \{T^{(b)}(h) = \sqrt{(T_1(h)^{(b)})^2 + (T_2(h)^{(b)})^2}\},$$

where  $T_m(h)^{(b)} = \frac{W^{(b)}(h+G) - 2W^{(b)}(h) + W^{(b)}(h-G)}{\sqrt{2G}}$  for  $m = 1, 2$ , and  $W^{(b)}(t)$  denotes a standard random walk at time  $t$ . The bandwidth set  $\mathcal{G}$  is defined as a grid ranging from 25 up to  $\min((n-1)/2, 200)$ . We use  $B = 1000$ . Then the threshold  $D_n(G, \alpha)$  is determined as the  $100(1-\alpha)^{\text{th}}$  percentile of  $\{D_n(G, \alpha)^{(b)}\}$ , which is compared to the Mahalanobis distance in (9). The initial change points (called initial candidates) are thus identified by collecting all  $k$  such that

$$D_{X^2}^2(k) > D_n(G, \alpha).$$

Finally, from the initial set of candidate points, we determine the finalized change points. MOSUM-type approaches are known to often detect an excessive number of change points due to the scaling (i.e.,  $\bar{S}_X(k)$ ) of the detectors (e.g., Eichinger and Kirch, 2018, Meier et al., 2021). To mitigate over-detection, the final change points are selected as the local maxima of the following expression for a small  $\eta \in (0, 1)$ :

$$\hat{k} = \underset{\hat{k}-\eta G \leq k \leq \hat{k}+\eta G}{\operatorname{argmax}} D_{X^2}^2(k),$$

In practice, we set  $\eta = 0.2$  when numerous change points are expected, such as in simulation studies where  $n$  is relatively small compared to  $G$ , which often occurs in our context. A smaller value of  $\eta$  generally increases detection sensitivity. The same procedure is applied to the other series  $\{Y_t\}$ .

### 3.3 Finding Simultaneous Change Points in Bivariate Series

Using the Joint-MOSUM approach described in Section 3.2, we extend the method to detect simultaneous changes across multiple series, referred to as Bi-MOSUM. Applying Joint- and Bi-MOSUM to both  $\{X_t\}$  and  $\{Y_t\}$  together and combining the result allows us to identify different types of combined cross-changes. It is worth noting that Joint- and Bi-MOSUM-type algorithms can be

readily extended to detect other types of changes (e.g., in autocovariances), which is beyond the scope of the study.

Suppose a pair of  $\{Y_t\}_{t=1}^n$  and  $\{X_t\}_{t=1}^n$  is given. For each combination of local cross-changes, it is equivalent to test one of the following four hypotheses at each time  $t = k$ :

$$\begin{aligned}
H_0(k) &: \mu_Y(k - G, k) = \mu_Y(k + 1, k + G), \quad \mu_X(k - G, k) = \mu_X(k + 1, k + G), \\
H_0(k) &: \mu_Y(k - G, k) = \mu_Y(k + 1, k + G), \quad \sigma_X^2(k - G, k) = \sigma_X^2(k + 1, k + G), \\
H_0(k) &: \sigma_Y^2(k - G, k) = \sigma_Y^2(k + 1, k + G), \quad \mu_X(k - G, k) = \mu_X(k + 1, k + G), \\
H_0(k) &: \sigma_Y^2(k - G, k) = \sigma_Y^2(k + 1, k + G), \quad \sigma_X^2(k - G, k) = \sigma_X^2(k + 1, k + G),
\end{aligned} \tag{10}$$

with the corresponding alternative hypothesis  $H_A(k)$  of each null hypothesis in (10) as the negation of  $H_0(k)$ . This indicates that either the features of  $Y_t$ ,  $X_t$ , or both have locally changed around the time point  $t = k$ . Again, we will suppress the window size  $G$  in both population and sample features' representation.

Specifically, consider a change in the mean of  $Y_t$  alongside a change in the variance of  $X_t$  as an example. The joint detector for this combination of changes at time  $t = k$  is defined as

$$J_{YX^2}(k) = \begin{pmatrix} T_Y^{(1)}(k) \\ T_X^{(2)}(k) \end{pmatrix} \in \mathbb{R}^2.$$

We then define the dependence between the mean of  $\{Y_t\}$  and the variance of  $\{X_t\}$  as

$$\Gamma_{YX^2} = \begin{pmatrix} 1 & \rho_{YX^2} \\ \rho_{YX^2} & 1 \end{pmatrix},$$

where

$$\rho_{YX^2} := \frac{\mathbb{E}[(Y - \mu_Y)(X - \mu_X)^2]}{\sqrt{\text{Var}(Y - \mu_Y)}\sqrt{\text{Var}((X - \mu_X)^2)}} := \frac{\sigma_{YX^2}^2}{\sigma_Y \nu_X}.$$

Its local sample analog around the time point  $t = k$ , denoted by  $\hat{\Gamma}_{YX^2}(k)$ , is computed as

$$\hat{\rho}_{YX^2}(k) = \frac{\bar{\sigma}_{XY^2}^2(k)}{\bar{S}_Y(k)\bar{V}_X(k)},$$

where  $\bar{S}_Y(k)$  and  $\bar{V}_X(k)$  are locally averaged variance and kurtosis defined in (5) and (7), respectively, and  $\bar{\sigma}_{XY^2}^2(k) = \frac{1}{2}(\hat{\sigma}_{XY^2}^2(k + 1, k + G) + \hat{\sigma}_{XY^2}^2(k - G + 1, k))$  denotes the locally averaged estimated cross-covariance at  $t = k$ , with

$$\hat{\sigma}_{XY^2}^2(a, b) = \frac{1}{b - a + 1} \sum_{t=a}^b (Y_t - \bar{Y}(a, b))(X_t - \bar{X}(a, b))^2.$$

That is, the local dependence between  $Y_t$  and  $X_t$  is considered when investigating their distributional shifts around the time point  $t = k$ . Finally, the Mahalanobis distance used to detect the combined local change at time  $t = k$  is computed as

$$D_{YX^2}^2(k) = J_{YX^2}(k)' \hat{\Gamma}_{YX^2}(k)^{-1} J_{YX^2}(k). \tag{11}$$

Note that we can also consider the other three combinations of local cross-distributional shifts described in (10), where the corresponding Mahalanobis distances are denoted as  $D_{YX}^2(k)$ ,  $D_{Y^2X}^2(k)$ , and  $D_{Y^2X^2}^2(k)$ ,  $k = 1, 2, \dots, n$ , defined analogously to (11).

Analogous to the Joint-MOSUM procedure, the Mahalanobis distance in (11) is compared with the same threshold  $D_n(G, \alpha)$

$$D_{YX^2}^2(k) > D_n(G, \alpha), \quad k = 1, \dots, n.$$

to determine whether the time points  $t = k$ ,  $k = 1, \dots, n$ , are initial candidate change points. Finally, the same screening rule as in the Joint-MOSUM procedure is applied; for a small  $\eta \in (0, 1)$ : we obtain

$$\hat{k} = \underset{\hat{k} - \eta G \leq k \leq \hat{k} + \eta G}{\operatorname{argmax}} D_{YX^2}^2(k).$$

The remaining three combined hypothesis tests for local cross-changes are performed similarly.

## 4 Identifying Hotspots

We construct hotspots as intervals around the identified time points and merge them into regions that capture both simultaneous and possibly asynchronous changes across the two series. This ensemble approach not only detects intervals of individual changes but also reveals potential interactions and associations between the series, without the need for explicit parametric modeling of their relationships.

### 4.1 Thresholding Rule

We report the union of time intervals for which the corresponding Mahalanobis distances exceed the given threshold. Note that the thresholds are the same for all types of joint detectors.

Continuing from the previous example, consider detecting simultaneous change points in the mean and variance of  $\{Y_t\}$  and  $\{X_t\}$ . The hotspot is defined as the set of times for which both distances  $D_Y^2(k)$  and  $D_{YX^2}^2(k)$  exceed the threshold  $D_n(G, \alpha)$ :

$$\hat{\mathcal{H}}_{thrs} := \left\{ k \in \{1, \dots, n\} : \underbrace{D_{YX^2}^2(k) > D_n(G, \alpha), D_Y^2(k) > D_n(G, \alpha)}_{(*)} \right\}. \quad (12)$$

Any other combinations of the Mahalanobis distance pairs with  $D_{YX}^2(k), D_{YX^2}^2(k), D_{Y^2X}^2(k)$ , and  $D_{Y^2X^2}^2(k)$  can be considered. For instance, if the goal is to detect all types of changes (in case of no prior knowledge), the condition (\*) on simultaneous changes in (12) is replaced with

$$\max(D_{YX}^2(k), D_{YX^2}^2(k), D_{Y^2X}^2(k), D_{Y^2X^2}^2(k)) > D_n(G, \alpha). \quad (13)$$

Likewise, depending on the choice of interest or our prior knowledge, this condition (13) can be substituted with other combinations of the comparisons between distances and the threshold. We refer to the procedure defined in (12) as the thresholding rule.

### 4.2 Confidence Interval Rule

CPD algorithms are designed to detect abrupt shifts rather than gradual transitions. Therefore, it is necessary to transform the estimated change points into intervals that capture both the detected locations and their neighboring regions, which requires quantifying the uncertainty associated with

each estimate and expressing it through confidence intervals. While extensive research has focused on developing CPD algorithms, relatively few studies have addressed uncertainty quantification, aside from a few Bayesian approaches (e.g., Belitser and Ghosal, 2025, Cappello and Madrid Padilla, 2025). In the frequentist approaches, methods based on controlling the family-wise error rate (Frick et al., 2014), false discovery rate (Li et al., 2016), and post-selection inference (Hyun et al., 2016) have been proposed. However, these approaches still produce discrete point estimates rather than intervals and thus fail to adequately capture the uncertainty or gradual transitions often observed in practice, as illustrated in Figure 1.

Recently, Cho and Kirch (2022) proposed two methods for constructing confidence intervals for change points in univariate MOSUM: one based on pointwise coverage and the other on controlling the family-wise error rate. However, our empirical results show that the latter often produces overly narrow intervals, which is undesirable in our context where overlapping regions between different types of changes need to be preserved. Therefore, we adopt the pointwise method in our framework.

Confidence intervals for change points from the Joint- and Bi-MOSUM procedures can be constructed in the same way as for univariate MOSUM change points, following the bootstrap approach in Section 2.3 of Cho and Kirch (2022) and Section 2.7 of Meier et al. (2021). The main idea is to create hotspots by merging these confidence intervals across different types of detected changes.

Continuing from the previous example, suppose there are  $\hat{K} = |\hat{\mathcal{T}}_{YX^2}|$  estimated change points corresponding to detected changes in the mean of  $Y_t$  and the variance of  $X_t$ . We order them as  $1 = \hat{k}_{YX^2,0} \leq \hat{k}_{YX^2,1} \leq \dots \leq \hat{k}_{YX^2,\hat{K}_j} \leq \hat{k}_{YX^2,\hat{K}_j+1} = n$ . Define each segment as  $I_j = \{\hat{k}_{j-1} + 1, \dots, \hat{k}_j\}$ ,  $j = 1, \dots, \hat{K} + 1$ . From each segment, we draw a random sample of size  $|I_j|$  from  $\{(Y_t, X_t) : t \in I_j\}$  and repeat this procedure  $B$  times (we use  $B = 1000$ ). This yields bootstrap samples  $\{(Y_1^{(b)}, X_1^{(b)}), \dots, (Y_n^{(b)}, X_n^{(b)})\}$ ,  $b = 1, \dots, B$ . For each bootstrap replication, the estimated change point is recalculated as

$$\hat{k}_{YX^2,j}^{(b)} = \underset{\hat{k}_{YX^2,j}-G \leq k \leq \hat{k}_{YX^2,j}+G}{\operatorname{argmax}} D_{YX^2}^{(b)}(k).$$

Next, for each  $\hat{k}_{YX^2,j}$ , we compute  $M_{YX^2,j}(\alpha)$  as the  $100(1 - \alpha)^{\text{th}}$  percentile of the absolute deviations  $|\hat{k}_j^{(1)} - \hat{k}_j|, \dots, |\hat{k}_j^{(B)} - \hat{k}_j|$ . The resulting pointwise  $100(1 - \alpha)\%$  confidence interval is then given by

$$\text{CI}_{YX^2,j}(\alpha) = [\hat{k}_j^{(b)} - M_{YX^2,j}(\alpha), \hat{k}_j^{(b)} + M_{YX^2,j}(\alpha)], \quad j = 1, \dots, \hat{K}.$$

Using these intervals, the hotspots are defined as

$$\hat{\mathcal{H}}_{CI}(\alpha) := \left\{ k = \{1, \dots, n\} : k \in \underbrace{\left( \bigcup_j \text{CI}_{YX^2,j}(\alpha) \right)}_{(**)} \cap \left( \bigcup_i \text{CI}_{Y,i}(\alpha) \right) \right\}. \quad (14)$$

Similar to the thresholding rule, if all types of changes are considered, the condition  $(**)$  is replaced by the union of intervals from all detector combinations:

$$\left( \bigcup_{j_1} \text{CI}_{YX,j_1}(\alpha) \right) \cup \left( \bigcup_{j_2} \text{CI}_{YX^2,j_2}(\alpha) \right) \cup \left( \bigcup_{j_3} \text{CI}_{Y^2X,j_3}(\alpha) \right) \cup \left( \bigcup_{j_4} \text{CI}_{Y^2X^2,j_4}(\alpha) \right). \quad (15)$$

Note that this condition (15) can be replaced with other combinations of confidence intervals. We refer to the procedure defined in (14) as the confidence interval rule.

### 4.3 Illustration of Algorithm

Two illustrative examples of hotspot identification are shown in Figures 2 and 3, provided in Appendix A.

The first example in Figure 2 shows a scenario in which the stress level series  $\{Y_t\}$  undergoes a single change in its mean, while the corresponding passive sensing variable exhibits simultaneous changes in both its mean and variance, with a five-time-point lag between the two series. The second example in Figure 3 demonstrates a case where the variance of the stress level changes twice, accompanied by two corresponding changes in the passive sensing variable, each occurring with a similar five-time-point lag. Furthermore, transforming the categorical stress-level series  $\{Y_t\}$  into a continuous form using (1) shows that the characterization of mean and variance shifts in the categorical distributions is preserved after the transformation described in Section 3.1. This is illustrated in Figure 2, which captures mean shifts, and Figure 3, which detects variance changes.

## 5 Numerical Studies

The numerical studies consist of three parts. First, we empirically demonstrate that jointly detecting multiple types of changes yields better performance than detecting each type individually, particularly when different types of changes coexist. At this stage, we also compare the proposed algorithm with benchmark methods to show that the Joint- and Bi-MOSUM-based approaches outperform alternative methods. Moreover, unlike typical numerical comparisons in the CPD literature, our primary interest lies in evaluating whether the algorithms can identify time points close to the true change locations, even if the detected timings are not exact, rather than assessing their precision in pinpointing exact change times.

Second, we examine how effectively the three proposed methods capture distributional shifts in a manner that is both concise and comprehensive. Specifically, we evaluate the hotspot definitions in terms of their ability to convey information efficiently, that is, by using shorter intervals without missing true changes, particularly in the presence of asynchronous changes across series. It is important to note that this experiment aims to explore the properties of the defined hotspots rather than to determine which definition is superior.

Finally, we apply the proposed rules to real-world data to illustrate their practical utility and interpretability in applied settings.

### 5.1 Simulation on Change Points

First, we focus on a univariate time series of interest. Throughout the simulation studies, the sample size is fixed at  $n = 100$ , as the lengths of passive sensing variables and stress-level series are typically not sufficiently long. We consider scenarios in which the number of change points ranges from one to three, located at  $k^* = 50$  for a single change,  $k^* = 40, 60$  for two changes, and  $k^* = 25, 50, 75$  for three changes. For each scenario, we examine six cases (Cases 1–6), each corresponding to a different signal strength. Case 1 represents the strongest signal (where the jump sizes are generally larger and the range of the noise is narrower and lower), while Case 6 corresponds to the weakest. The signal strength is controlled by varying the magnitude of the mean shift, denoted by  $(-\mu, \mu)$ , and by adjusting the variance across segments from  $\sigma_{\min}$  to  $\sigma_{\max}$ .

The parameter settings are as follows:

- Case 1:  $\mu = 2, \sigma_{\min} = 0.1, \sigma_{\max} = 0.4,$
- Case 2:  $\mu = 2, \sigma_{\min} = 0.1, \sigma_{\max} = 0.8,$
- Case 3:  $\mu = 2, \sigma_{\min} = 0.4, \sigma_{\max} = 0.8,$
- Case 4:  $\mu = 1, \sigma_{\min} = 0.1, \sigma_{\max} = 0.4,$
- Case 5:  $\mu = 1, \sigma_{\min} = 0.1, \sigma_{\max} = 0.8,$
- Case 6:  $\mu = 1, \sigma_{\min} = 0.4, \sigma_{\max} = 0.8.$

Each setting is replicated 500 times.

We use the Joint-MOSUM method described in Section 3 with window sizes  $G = 20$  and  $G = 40$ . These two settings are compared against several established univariate CPD algorithms. Specifically, we include PELT by Killick et al. (2012) implemented in the R package `changePoint` (Killick and Eckley, 2014), `stepR` by Pein et al. (2017), and wild binary segmentation (WBS) by Fryzlewicz (2014), implemented in the R package `breakfast`. In addition, we use the univariate MOSUM algorithm proposed by Eichinger and Kirch (2018), implemented in the R package `mosum`, with the same window sizes ( $G = 20, 40$ ). All benchmark methods considered are widely used, have demonstrated strong performance across various contexts, and are publicly accessible. Note that, however, the goal of the comparison is to emphasize the necessity and suitability of the proposed CPD algorithm for the type of data analyzed in this study, rather than pinpointing the estimation accuracy.

For performance evaluation, we use power and false discovery rate (FDR), defined as follows. For each replication  $i = 1, \dots, 500$ , and let  $\hat{K}^{(i)}$  denote the number of detected change points at the  $i^{\text{th}}$  iteration. Then,

$$\text{Power}(\eta) = \frac{1}{500} \sum_{i=1}^{500} 1_{\{\cap_{\ell=1}^{K^*} [\cup_{j=1}^{\hat{K}^{(i)}} \{t_j^{(i)} - t_\ell^* \leq \eta\}]\}}, \quad (16)$$

$$\text{FDR}(\eta) = \frac{\sum_{i=1}^{500} 1_{\{\{\hat{K}^{(i)} \geq 1\} \& \{\cap_{\ell=1}^{K^*} [\cup_{j=1}^{\hat{K}^{(i)}} \{|t_j^{(i)} - t_\ell^*| > \eta\}]\}}}{\sum_{i=1}^{500} 1_{\{\hat{K}^{(i)} \geq 1\}}}, \quad (17)$$

where  $K^*$  is the number of true change points. We set  $\eta = 5$  to evaluate whether each true change point (or each pair of start and end points if there are multiple true change points) is correctly identified within a specified tolerance range, regardless of the number of detected alarms within that region. Throughout all simulations, the significance level is fixed at  $\alpha = 0.05$ .

Table 1 presents the simulation results. When different types of changes coexist, the Joint-MOSUM method generally exhibits superior performance across the evaluated metrics. This finding emphasizes the necessity and suitability of the proposed CPD algorithm for the type of data analyzed in this study, where the simultaneous changes occur even in a single time series. For all methods, including the proposed approach, performance tends to decline as the scenarios become more challenging, such as when the jump sizes are smaller, the variance ranges are narrower, or the overall variance level is higher. In a few cases, a slight improvement is observed when moving from Case 3 to Case 4; however, this pattern is not consistent across settings.

When there is only a single change point, a larger window size ( $G = 40$ ) yields better results. In contrast, when multiple change points are present, shorter windows perform better because the distance between change points is relatively small and the total sample size is shorter than what

	Power(5)						FDR(5)					
# of jumps: 1	Case 1	Case 2	Case 3	Case 4	Case 5	Case 6	Case 1	Case 2	Case 3	Case 4	Case 5	Case 6
Joint-MOSUM ( $G = 20$ )	<b>0.904</b>	<b>0.888</b>	<b>0.780</b>	0.834	0.766	<b>0.632</b>	0.020	<b>0.024</b>	0.064	0.048	0.064	0.098
Joint-MOSUM ( $G = 40$ )	0.910	<b>0.888</b>	0.762	<b>0.860</b>	<b>0.810</b>	0.612	0.022	0.042	0.088	0.042	0.090	0.118
PELT	0.898	0.880	0.712	0.812	0.766	0.510	0.096	0.118	0.286	0.180	0.226	0.490
stepR	0.872	0.822	0.734	0.768	0.662	0.528	0.026	0.058	<b>0.034</b>	0.050	0.128	0.064
WBS	0.892	0.846	0.770	0.808	0.694	0.594	0.108	0.154	0.230	0.192	0.306	0.406
MOSUM ( $G = 20$ )	0.866	0.798	0.718	0.748	0.628	0.508	<b>0.018</b>	0.026	0.038	<b>0.036</b>	<b>0.028</b>	<b>0.052</b>
MOSUM ( $G = 40$ )	0.878	0.828	0.762	0.804	0.676	0.584	0.024	0.034	0.052	0.052	0.072	0.092
# of jumps: 2	Case 1	Case 2	Case 3	Case 4	Case 5	Case 6	Case 1	Case 2	Case 3	Case 4	Case 5	Case 6
Joint-MOSUM ( $G = 20$ )	<b>0.850</b>	<b>0.756</b>	<b>0.648</b>	<b>0.674</b>	<b>0.580</b>	<b>0.380</b>	<b>0.002</b>	<b>0.008</b>	<b>0.016</b>	<b>0.012</b>	<b>0.025</b>	0.066
Joint-MOSUM ( $G = 40$ )	0.260	0.234	0.226	0.238	0.220	0.142	0.032	0.043	0.068	0.045	0.067	0.118
PELT	0.000	0.000	0.000	0.000	0.000	0.000	0.028	0.070	0.172	0.096	0.196	0.452
stepR	0.756	0.566	0.436	0.504	0.304	0.144	0.010	0.029	0.032	0.025	0.090	0.088
WBS	0.824	0.654	0.594	0.608	0.442	0.296	0.016	0.034	0.062	0.040	0.140	0.230
MOSUM ( $G = 20$ )	0.768	0.580	0.522	0.538	0.354	0.264	<b>0.002</b>	0.010	0.021	0.015	0.045	<b>0.049</b>
MOSUM ( $G = 40$ )	0.108	0.088	0.088	0.100	0.056	0.056	0.012	0.025	0.032	0.031	0.084	0.106
# of jumps: 3	Case 1	Case 2	Case 3	Case 4	Case 5	Case 6	Case 1	Case 2	Case 3	Case 4	Case 5	Case 6
Joint-MOSUM ( $G = 20$ )	<b>0.796</b>	<b>0.654</b>	<b>0.504</b>	<b>0.616</b>	<b>0.414</b>	<b>0.248</b>	<b>0.000</b>	<b>0.002</b>	<b>0.002</b>	<b>0.002</b>	<b>0.012</b>	<b>0.014</b>
Joint-MOSUM ( $G = 40$ )	0.142	0.136	0.094	0.126	0.074	0.034	0.018	0.040	0.039	0.034	0.075	0.109
PELT	0.000	0.000	0.000	0.000	0.000	0.000	0.010	0.038	0.118	0.064	0.236	0.443
stepR	0.602	0.448	0.236	0.366	0.162	0.032	0.004	0.014	0.022	0.020	0.045	0.082
WBS	0.700	0.546	0.420	0.504	0.258	0.166	0.002	0.010	0.028	0.012	0.076	0.096
MOSUM ( $G = 20$ )	0.682	0.494	0.386	0.462	0.212	0.140	0.002	0.006	0.006	0.004	0.026	0.022
MOSUM ( $G = 40$ )	0.010	0.004	0.004	0.008	0.004	0.000	0.014	0.034	0.043	0.034	0.095	0.115

Table 1: Power and FDR for  $\eta = 5$  based on simulation results using Joint-MOSUM and other benchmarks under three scenarios of a univariate series, each with six different signal strengths (Cases). A significance level of  $\alpha = 0.05$  is used if required for some CPD methods. The best performance in each scenario is shown in bold.

is typically considered in the CPD literature. Although shorter window sizes tend to generate more false alarms, it can be acceptable in the context of stress detection, where type-I errors, i.e., false notifications of stress when none is present, are generally less critical than missed detections. Hence, using shorter windows can be advantageous in such applications.

For the next simulation studies, we ensemble the four combinations of the Bi-MOSUM results and compare them with other CPD algorithms for bivariate series. Similar to the univariate case, the sample size for each of the two series is fixed at  $n = 100$ . We consider six different cases consistent with the univariate simulation setups. For each pair of series, distributional changes are introduced under the following scenarios: (i) a change at  $k^* = 40$  in the first series and  $k^* = 60$  in the second series, (ii) a change at  $k^* = 50$  in the first series and  $k^* = 40, 60$  in the second series, and (iii) changes at  $k^* = 40, 60$  in the first series and  $k^* = 30, 70$  in the second series. Each setup is replicated 500 times.

For Bi-MOSUM, we run four types of combinations (mean–mean, mean–variance, variance–mean, and variance–variance) to simulate scenarios in which the types of distributional changes are not known in advance, and then merge the estimated change points. We use window sizes  $G = 20$  and  $G = 40$  for the algorithm. Although most CPD algorithms are designed for univariate data, several multivariate CPD methods have been widely validated in different contexts. Specifically, we consider the nonparametric multivariate CPD by Matteson and James (2014), implemented in the R package `ecp` (James and Matteson, 2015); sparsified binary segmentation by Cho and Fryzlewicz (2015); and the double cumulative sum (CUSUM) statistic by Cho (2016), both implemented in the

	Power( $\eta=5$ )						FDR( $\eta=0$ )					
# of jumps: (1,1)	Case 1	Case 2	Case 3	Case 4	Case 5	Case 6	Case 1	Case 2	Case 3	Case 4	Case 5	Case 6
Bi-MOSUM ( $G = 20$ )	0.844	0.782	0.608	0.734	0.602	0.398	0.050	0.118	0.209	0.132	0.252	0.447
Bi-MOSUM ( $G = 40$ )	<b>0.968</b>	<b>0.912</b>	<b>0.830</b>	<b>0.910</b>	<b>0.772</b>	<b>0.552</b>	<b>0.024</b>	<b>0.036</b>	<b>0.090</b>	<b>0.066</b>	<b>0.101</b>	<b>0.241</b>
ecp	0.166	0.166	0.072	0.130	0.116	0.024	0.129	0.288	0.337	0.267	0.428	0.573
SBS	0.786	0.688	0.482	0.606	0.422	0.208	0.063	0.110	0.221	0.152	0.335	0.458
DCBS	0.018	0.028	0.008	0.018	0.042	0.022	0.980	0.935	0.947	0.953	0.911	0.880
NMP	0.734	0.682	0.612	0.578	0.448	0.426	0.092	0.154	0.251	0.198	0.409	0.535
# of jumps: (1,2)	Case 1	Case 2	Case 3	Case 4	Case 5	Case 6	Case 1	Case 2	Case 3	Case 4	Case 5	Case 6
Bi-MOSUM ( $G = 20$ )	<b>0.956</b>	<b>0.842</b>	<b>0.722</b>	<b>0.818</b>	<b>0.686</b>	<b>0.436</b>	<b>0.012</b>	<b>0.032</b>	0.085	0.048	0.125	0.289
Bi-MOSUM ( $G = 40$ )	0.714	0.558	0.556	0.618	0.400	0.260	<b>0.012</b>	0.018	<b>0.046</b>	<b>0.034</b>	<b>0.091</b>	<b>0.209</b>
ecp	0.000	0.002	0.000	0.000	0.004	0.000	0.133	0.236	0.375	0.315	0.424	0.544
SBS	0.344	0.322	0.136	0.236	0.166	0.070	0.048	0.105	0.229	0.179	0.266	0.474
DCBS	0.000	0.000	0.000	0.002	0.000	0.002	0.964	0.954	0.915	0.938	0.902	0.849
NMP	0.232	0.182	0.160	0.146	0.136	0.090	0.050	0.122	0.180	0.176	0.351	0.452
# of jumps: (2,2)	Case 1	Case 2	Case 3	Case 4	Case 5	Case 6	Case 1	Case 2	Case 3	Case 4	Case 5	Case 6
Bi-MOSUM ( $G = 20$ )	<b>0.928</b>	<b>0.840</b>	<b>0.696</b>	<b>0.778</b>	<b>0.590</b>	<b>0.338</b>	<b>0.002</b>	0.012	0.028	0.020	0.068	0.196
Bi-MOSUM ( $G = 40$ )	0.431	0.358	0.282	0.320	0.204	0.084	<b>0.002</b>	<b>0.004</b>	<b>0.026</b>	<b>0.012</b>	<b>0.046</b>	<b>0.140</b>
ecp	0.000	0.000	0.000	0.000	0.000	0.000	0.081	0.185	0.247	0.190	0.390	0.461
SBS	0.184	0.078	0.044	0.068	0.028	0.004	0.020	0.089	0.115	0.092	0.248	0.391
DCBS	0.012	0.022	0.012	0.010	0.020	0.016	0.968	0.928	0.912	0.932	0.878	0.872
NMP	0.002	0.004	0.008	0.008	0.004	0.008	0.020	0.072	0.120	0.100	0.269	0.355

Table 2: Power for  $\eta = 5$  and FDR for  $\eta = 0$  based on simulation results using Bi-MOSUM and other benchmarks under three scenarios of bivariate series, each with six different signal strengths (Cases). A significance level of  $\alpha = 0.05$  is used if required for some CPD methods. The best performance in each scenario is shown in bold.

R package `hdbinseg`. Additionally, we include a nonparametric CPD algorithm by Padilla et al. (2021), which is implemented independently of the authors<sup>‡</sup>.

Similar to the univariate simulation setup, we evaluate performance using power (16) and FDR (17), with  $\eta = 5$  for power and  $\eta = 0$  for FDR, since allowing a tolerance for FDR would make the performance of different methods indistinguishable. Here, the true and estimated change points from both series are merged separately. For example,  $K^* = 3$  when there is one true change point in one series and two in the other.

Table 2 presents the simulation results. The results generally mirror the patterns observed in the univariate series: as the signal strength decreases, the performance of all methods deteriorates, and more change points lead to further challenges. Nevertheless, the proposed method remains robust across all scenarios. Similar trends regarding the choice of window sizes, as seen in the univariate simulations, are also observed here. Throughout the simulation studies, the results demonstrate the necessity and effectiveness of ensembling detection results from MOSUM-type algorithms to accurately anchor the change points initially.

## 5.2 Simulation on Hotspots

We evaluate the hotspot definitions based on their ability to convey information efficiently, using shorter intervals while still capturing the true change points, particularly in the presence of asynchronous changes across series.

We apply two rules: the thresholding rule (Thrs), defined in (12), and the confidence interval (CI) rule, defined in (14) with  $\alpha = 0.05$ . The sample size is fixed at  $n = 100$ , and six cases with

<sup>‡</sup>The functioning code available at <https://github.com/HaotianXu/changepoints/tree/main>

doubled ranges of mean changes are considered, as described in Section 3. We examine a pair of time series,  $\{X_t\}$  and  $\{Y_t\}$ , which contain one and two change points, respectively. For  $\{X_t\}$ , the change points are located at  $k^* = 50$  and  $k^* = 40, 60$  for the two scenarios, while for  $\{Y_t\}$ , the change points are at  $k^* = 50 + \delta$  and  $k^* = 40 + \delta, 60 + \delta$ , with  $\delta \in \{0, 5\}$ . Each setting is repeated 500 times. For each replication, we apply the Joint- and Bi-MOSUM methods using window sizes  $G = 20$  and  $40$ . The hotspots are then computed according to their respective definitions, with (\*) and (\*\*) in (12) and (14) replaced by (13) and (15), respectively.

As a performance metric, we first consider the hit rate, defined as the proportion of trials (out of 500 replications) in which the identified hotspots include the true change points  $k^*$  in  $\{Y_t\}$ . For each replication, in the case of a single change point, a score of 1 is assigned if any identified hotspot contains  $k^*$ , and 0 otherwise. In the case of two change points, scores of 1, 0.5, or 0 are assigned according to the number of hits. Second, we consider the lengths of the continuous (non-segmented) intervals that include the true change points. Replications where no hotspots are identified are excluded from this calculation. If the identified hotspots fail to include the true change points in  $\{Y_t\}$ , a length of  $n = 100$  is assigned, indicating that the entire sample path would need to be reexamined. We report the averages of these two performance metrics across all replications.

Table 3 presents the simulation results. Overall, the thresholding rule produces wider hotspots compared to the confidence interval rule. As scenarios become more challenging, with lower signal strength, hit rates decline in most cases, with only a few exceptions. For the confidence interval rule, shorter window sizes are preferred because they achieve higher hit rates while maintaining relatively short intervals. This observation is consistent with the simulation studies on the CPD algorithms. In contrast, although longer window sizes improve hit rates for the thresholding rule, they tend to produce wide hotspot intervals, making it subtle to link distributional shifts in passive sensing variables to specific timings of changes of stress level.

Comparing cases with  $\delta = 0$  and  $\delta = 5$ , representing no and large asynchrony respectively, the thresholding rule remains relatively stable for a single jump, whereas the performance of the confidence interval rule tends to decline as the discrepancy increases. In scenarios with two jumps, hit rates generally remain stable across most conditions, with a few exceptions. As expected, for all cases and numbers of jumps, both hotspot definitions produce wider intervals as the asynchrony increases and the number of jumps grows.

Interestingly, the two rules exhibit reverse trends in response to signal strength. As scenarios become more challenging, intervals defined by the thresholding rule become narrower, while those defined by the confidence interval rule become wider. This occurs because, as the signal weakens, the Mahalanobis distance is less likely to exceed the threshold, reducing the temporal region flagged by the thresholding rule. Conversely, as the variance of the estimator increases, confidence intervals widen, and overlapping regions from multiple confidence intervals expand. Thus, each rule reflects the intrinsic properties of the underlying method from which it is derived.

### 5.3 Data Application

We apply the rules tested in Section 5.2 to the real data from the ALACRITY Phase I study, conducted by the Weill Cornell ALACRITY Center (P50MH113838). In this application, we focus on four patients, with their stress levels and one passive sensing variable for each shown in Figure 1. For each patient (sternrelief15, sternrelief16, sternrelief5, and sternrelief6), we select three different passive sensing variables from different sensors: step counts collected via the Pedometer app,

		Hit rate						Length of intervals					
1 jump in $\{Y_t\}$		Case 1	Case 2	Case 3	Case 4	Case 5	Case 6	Case 1	Case 2	Case 3	Case 4	Case 5	Case 6
$\hat{\mathcal{H}}$								$\delta = 0$					
Thrs	$G = 20$	0.958	0.910	0.864	0.904	0.858	0.740	28.080	25.471	23.872	25.413	21.088	18.036
	$G = 40$	0.974	0.964	0.918	0.946	0.926	0.818	57.805	49.568	45.440	48.538	40.033	35.383
CI	$G = 20$	0.944	0.916	0.888	0.914	0.872	0.788	1.294	2.175	2.628	2.236	4.013	6.907
	$G = 40$	0.848	0.804	0.872	0.830	0.736	0.784	1.375	1.778	2.515	1.901	3.743	6.859
$\hat{\mathcal{H}}$								$\delta = 5$					
Thrs	$G = 20$	0.956	0.902	0.876	0.912	0.842	0.728	28.431	25.114	24.685	24.550	20.160	17.844
	$G = 40$	0.976	0.936	0.918	0.944	0.916	0.812	59.492	51.872	50.051	50.126	40.966	36.963
CI	$G = 20$	0.736	0.628	0.594	0.556	0.504	0.494	3.036	3.227	2.888	2.601	4.138	5.946
	$G = 40$	0.298	0.304	0.270	0.264	0.290	0.348	1.337	1.767	2.000	1.706	3.606	6.311
2 jumps in $\{Y_t\}$		Case 1	Case 2	Case 3	Case 4	Case 5	Case 6	Case 1	Case 2	Case 3	Case 4	Case 5	Case 6
$\hat{\mathcal{H}}$								$\delta = 0$					
Thrs	$G = 20$	0.797	0.736	0.658	0.702	0.589	0.525	45.346	40.866	37.877	40.328	32.620	28.086
	$G = 40$	0.956	0.937	0.902	0.910	0.836	0.780	63.868	58.092	54.345	55.388	45.745	39.743
CI	$G = 20$	0.672	0.628	0.578	0.620	0.574	0.490	18.051	19.379	16.808	18.340	20.309	16.533
	$G = 40$	0.491	0.425	0.382	0.429	0.365	0.351	15.291	12.990	14.600	14.094	12.472	15.159
$\hat{\mathcal{H}}$								$\delta = 5$					
Thrs	$G = 20$	0.792	0.725	0.654	0.674	0.582	0.521	45.622	41.228	36.310	38.758	32.332	26.940
	$G = 40$	0.961	0.946	0.900	0.904	0.842	0.788	63.374	58.078	52.133	54.952	45.037	39.676
CI	$G = 20$	0.728	0.629	0.508	0.572	0.493	0.410	24.570	22.801	17.624	19.679	19.249	15.591
	$G = 40$	0.214	0.195	0.181	0.187	0.218	0.194	7.994	7.208	7.494	7.688	10.026	9.072

Table 3: Average hit rate and length of the intervals containing the true change points for the hotspots identified using the two definitions (Thresholding and confidence interval rules, respectively). A significance level of  $\alpha = 0.05$  is used for all steps.

conversation percentage collected via the VoicePresence app, and sleep duration collected via the AppDailyReport app, all of which were installed on patients’ smartphones. These variables represent different types of human behaviors, including physical activity, sociability, and sleep quality, which are strongly assumed to be associated with stress (e.g., Triantafyllou et al., 2019, daSilva et al., 2021, Baretta et al., 2025). Since the passively sensed variables operate on different scales, we analyze them in their original units without applying normalization. Stress levels were reported daily by the four patients using a 5-item Likert scale (1 = none, 5 = extremely high) via the same devices. The passive sensing variables were summarized on a daily basis to match the observation frequency of the stress measurements.

Table 4 presents the results of hotspot identification along with the corresponding estimated change points. Visualizations of the identified hotspots for each combination of passive sensing variables and stress levels are shown in Figures 4, 5, 6, and 7 in Appendix A. The locations of the hotspots closely align with those observed through visual inspection in Figure 1. Interestingly, the hotspots across different combinations of passive sensing variables and stress levels tend to be consistent.

In general, the change points identified in the stress levels are similar for both  $G = 20$  and  $G = 40$ , although the cross-change points vary. Using  $G = 40$  generally detects more change points than  $G = 20$ . Hotspots identified with the thresholding rule are considerably narrower than those obtained via the confidence interval rule, suggesting that the signal strength is relatively weak compared to the noise. Additionally, detections for  $YX$  and  $YX^2$  occur more frequently than for  $Y^2X$  and  $Y^2X^2$ , indicating that these changes are easier to detect. Overall, these results suggest that the signals in the passive sensing variables are generally weaker than those in the stress levels.

Patients	$G$	Variables	Change points					Hotspots	
			$Y$	$YX$	$YX^2$	$Y^2X$	$Y^2X^2$	Thrs	CI
sternreleif15	$G = 20$	SC	-	-	-	96	-	-	-
		CP	-	-	-	-	-	-	-
		SD	-	62	-	62	-	-	-
	$G = 40$	SC	59,81	63,82,109	82,93	101	-	[59,59],[81,83],[93,93]	[30,109]
		CP	59,81	81	63,82,93	-	62	[57,57],[59,59],[81,88],[91,93]	[38,107]
		SD	59,81	62,82,101,126	82,93	62,101,126	[57,57],[59,59],[81,82],[91,93]	[30,107]	-
sternreleif16	$G = 20$	SC	44,64	44,64	45,64	45,64	-	[43,47],[63,65],[87,87]	[24,83]
		CP	44,64	45,64	45,65	36,56	36,50,59	[43,52],[62,65],[87,87]	[24,83]
		SD	44,64	30,45,64	44,64	30,51	56	[43,52],[63,64],[87,87]	[24,83]
	$G = 40$	SC	44	-	-	-	-	-	-
		CP	44	-	45	-	-	[42,47],[87,87]	[10,98,77.03]
		SD	44	-	44	-	-	[44,45],[87,87]	[9,98,78.03]
sternreleif5	$G = 20$	SC	-	72,80	78,131	72,93,100	78	-	-
		CP	-	-	80,132	-	70	-	-
		SD	-	112,132	-	-	69	-	-
	$G = 40$	SC	79,96	50,77	83	50,77	83	[78,80],[88,88],[95,98]	[54,103]
		CP	79,96	52,79,91	80	50	72	[78,80],[88,88],[95,96]	[52.00,122.03]
		SD	79,96	49,78,112	78	49,72,112	72	[78,80],[88,88],[95,96]	[53,123]
sternreleif6	$G = 20$	SC	62	62	62	-	-	[53,70]	[52,72]
		CP	62	62	62,89	66	89	[53,70]	[52,72]
		SD	62	62	64	-	-	[53,70]	[53,71]
	$G = 40$	SC	54,63	54,63	9,54,63	-	9	[43,79]	[36,98,80.00]
		CP	54,63	54,63	54,63	69	70	[43,79]	[35,82]
		SD	54,63	54,63	54,63	-	-	[44,79]	[32.00,81.03]

Table 4: Results of the estimated change points (middle five columns) are shown for different types of changes, along with the identified hotspots (right two columns). Each of the four sections represents one patient, with three passive sensing variables considered per patient and for each window size,  $G = 20, 40$ . The abbreviations SC, CP, and SD in the variable names denote step counts, conversation percentage, and sleep duration, respectively. A significance level of  $\alpha = 0.05$  is used for all steps.

## 6 Discussion

In this article, we focus on the identification of hotspots, defined as collections of time intervals during which clinical experts are advised to monitor changes in features derived from passive sensing variables, reflecting variations in human behaviors. The proposed algorithm serves as an auxiliary tool for clinicians seeking to investigate the associations between stress and human behavior by tracking changes in these series. The method is based on the MOSUM-type CPD algorithms, designed to capture simultaneous changes in statistical features within or across given series. For the combined identified change points, the algorithm ensembles local neighborhoods using test statistics and constructs confidence intervals to define the hotspots.

The simulation studies were conducted in two stages. The first stage compared the proposed Joint- and Bi-MOSUM approaches with other CPD algorithms, demonstrating the necessity and suitability of MOSUM-type methods tailored to our specific time series. The second stage explored the properties of the hotspots defined by the two rules. The results show that the hotspots reflect the characteristics of the underlying methods from which they were derived. In the real data application, we illustrate changes in stress levels associated with passive sensing variables of interest. The identified hotspot regions are generally consistent across different passive sensing variables, although the detections are not solely driven by changes in stress, as the initially identified change points differ across series.

There are several limitations of the proposed method, which point to important directions for future work. First, the current framework has not yet been extended to multivariate settings. When the detected change points differ across multiple passive sensing variables, additional proce-

dures such as ranking-and-selection or ensemble-based integration would be required to consolidate the results. Second, a natural next step would be to develop a change point detection method that leverages the Mahalanobis distance for truly multivariate data, enabling simultaneous analysis across more than four detectors. However, such an extension would require new theoretical developments that are not yet available. Finally, the proposed method does not directly validate the associations between passive sensing variables and stress levels; it operates under the assumption that such associations exist. Future work should aim to incorporate models capable of formally testing and validating these relationships in clinical studies.

## 7 Software

The R code used for illustrating the method in Section 4.3 and for the simulation studies and data application in Section 5 is available on GitHub at <https://github.com/yk748/hotspot>.

## Acknowledgements

The data that support the findings of this study are available on request from the corresponding author. The data are not publicly available due to privacy or ethical restrictions.

## Funding

S. Banerjee acknowledges partial supports from NIMH award P50MH113838 and NIA award P01AG073090. S. Basu acknowledges partial support from NSF CAREER award DMS-2239102. In addition, S. Basu acknowledges partial support from NSF awards DMS-1812128, DMS-2210675, and NIH awards R01GM135926, R21NS120227.

## A Additional Figures

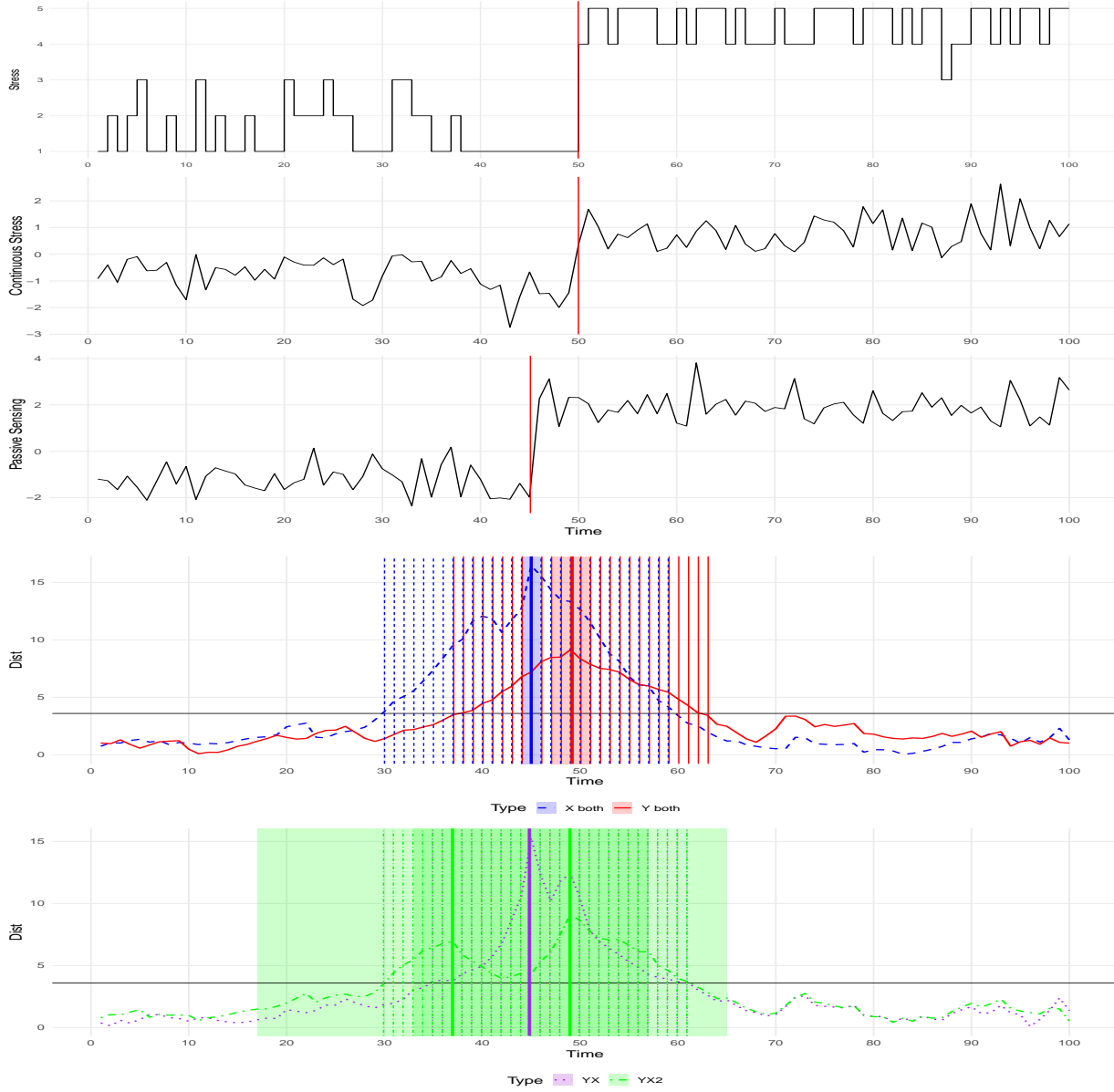


Figure 2: (Top) Time series plots of stress levels (first), their continuous counterparts ( $\{Y_t\}$ ; second), and the passive sensing variable ( $\{X_t\}$ ; third). The true change point of the stress level is at  $k^* = 50$ . (Bottom) Mahalanobis distances from the Joint-MOSUM of  $Y_t$  and  $X_t$  are shown in red and blue (first), and those from the Bi-MOSUM for mean changes in both  $Y_t$  and  $X_t$  (purple) and for a mean change in  $Y_t$  with a variance change in  $X_t$  (green). The thick vertical lines indicate the estimated change points from each MOSUM. The dashed vertical lines indicate the time points at which each distance exceeds the threshold (black), which is externally computed using a Monte Carlo simulation (slightly different from the one used in the MOSUM algorithm). The shaded areas represent pointwise confidence intervals. The hotspots are thus  $[37, 61]$  by the thresholding rule and  $[47, 51]$  by the confidence interval rule, respectively.

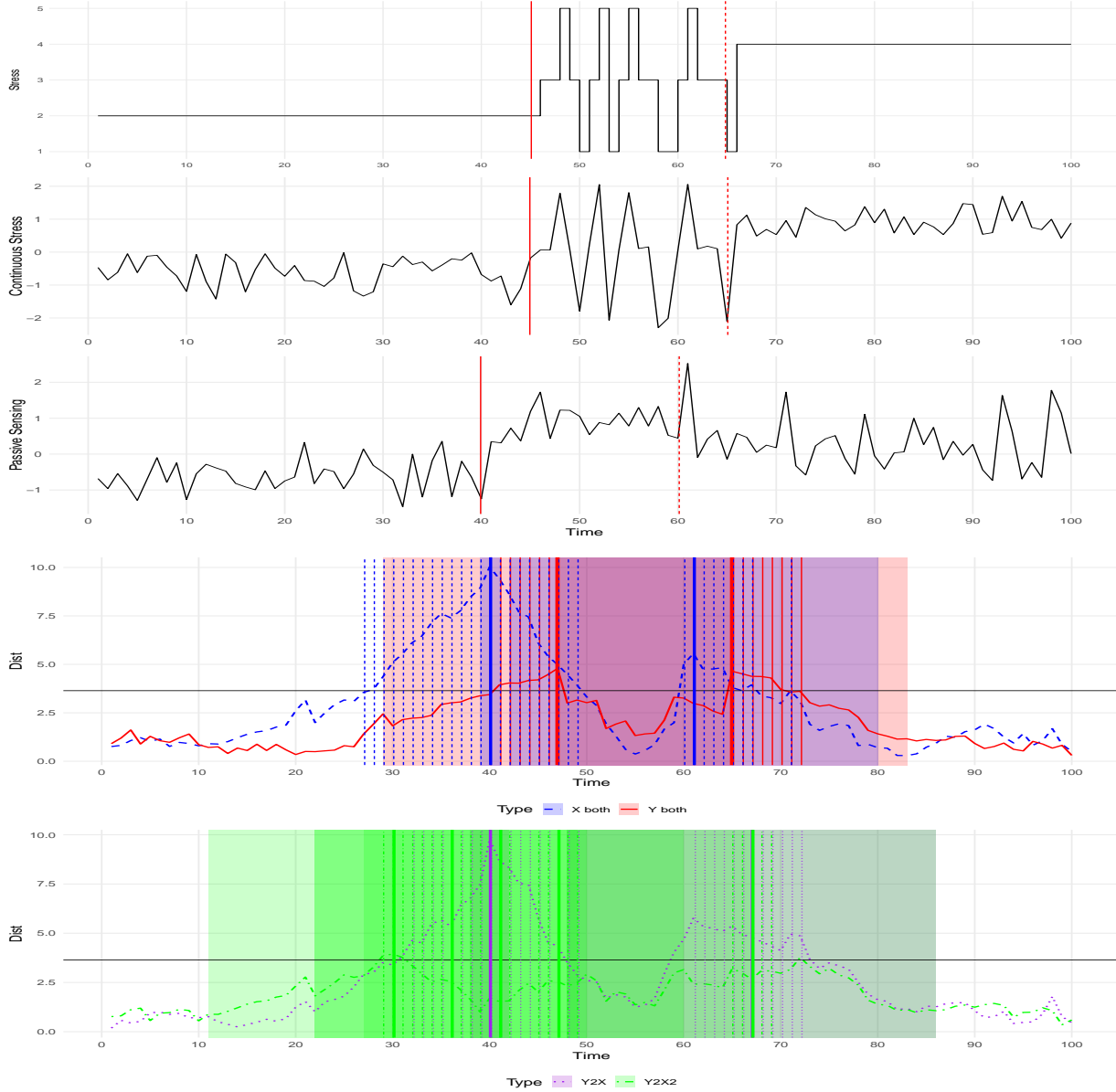


Figure 3: (Top) Time series plots of stress levels (first), their continuous counterparts ( $\{Y_t\}$ ; second), and the passive sensing variable ( $\{X_t\}$ ; third). The true change points of the stress level are at  $k^* = 40, 60$ . (Bottom) Mahalanobis distances from the Joint-MOSUM of  $Y_t$  and  $X_t$  are shown in red and blue (first), and those from the Bi-MOSUM for variance change in  $Y_t$  with a mean change in  $X_t$  (purple) and both variance changes in both  $Y_t$  and  $X_t$  (green). The thick vertical lines indicate the estimated change points from each MOSUM. The dashed vertical lines indicate the time points at which each distance exceeds the threshold (black), which is externally computed using a Monte Carlo simulation (slightly different from the one used in the MOSUM algorithm). The shaded areas represent uniform confidence intervals. The hotspots are thus  $[40, 47], [65, 72]$  by the thresholding rule and  $[29, 83]$  by the confidence interval rule, respectively.

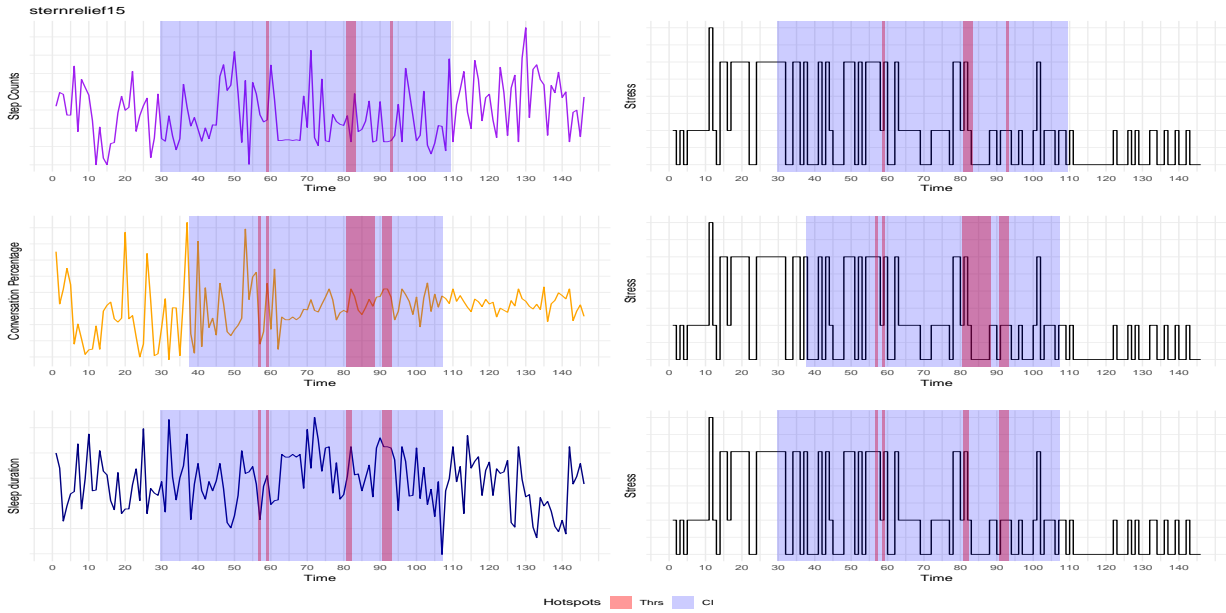


Figure 4: Results of the identified hotspots for sternrelief15 with  $G = 40$  across three combinations of passive sensing variables (left; step count, conversation percentage, and sleep duration in each row) and stress levels (right). The two definitions, threshold and confidence interval rules, are shown as red and blue shaded areas, respectively.

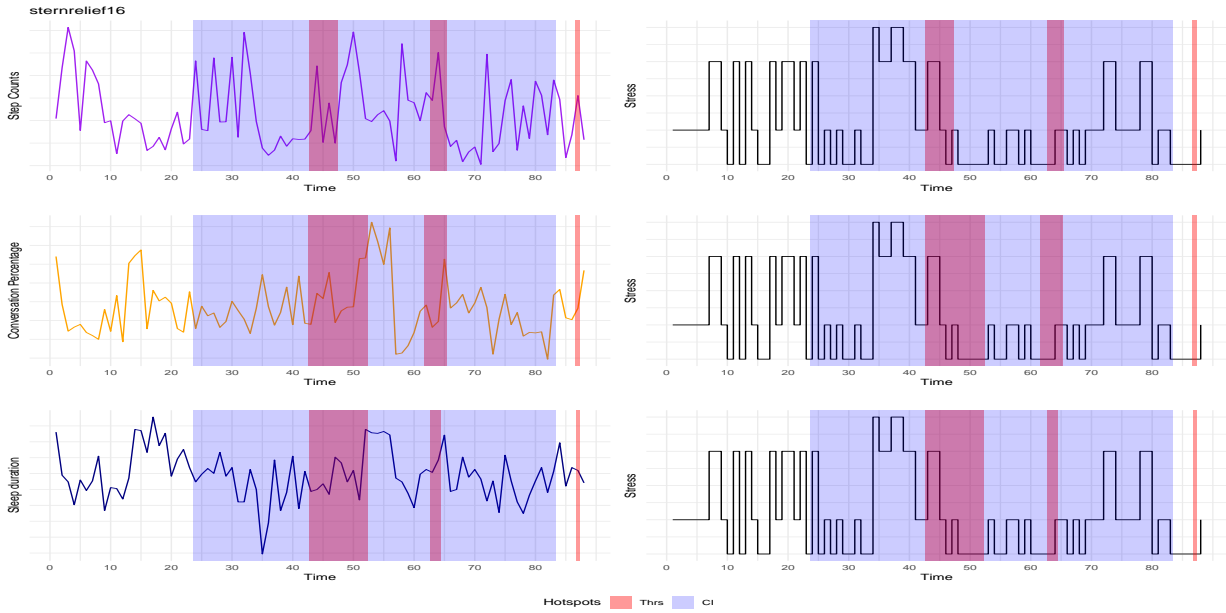


Figure 5: Results of the identified hotspots for sternrelief16 with  $G = 20$  across three combinations of passive sensing variables (left; step count, conversation percentage, and sleep duration in each row) and stress levels (right). The two definitions, threshold and confidence interval rules, are shown as red and blue shaded areas, respectively.

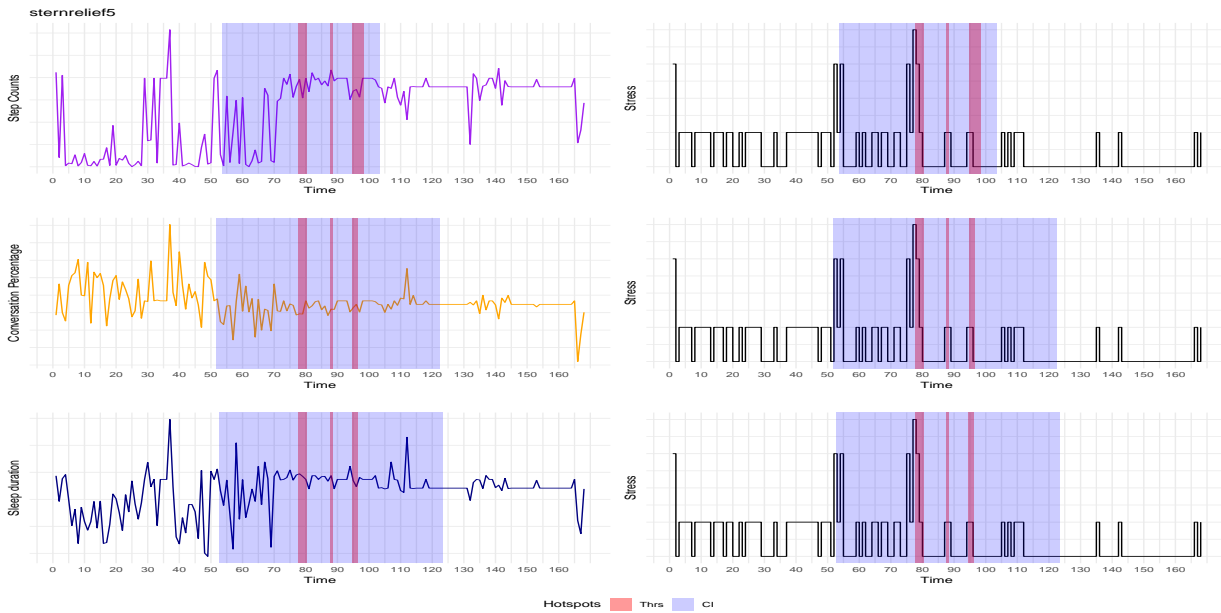


Figure 6: Results of the identified hotspots for sternrelief5 with  $G = 40$  across three combinations of passive sensing variables (left; step count, conversation percentage, and sleep duration in each row) and stress levels (right). The two definitions, threshold and confidence interval rules, are shown as red and blue shaded areas, respectively.

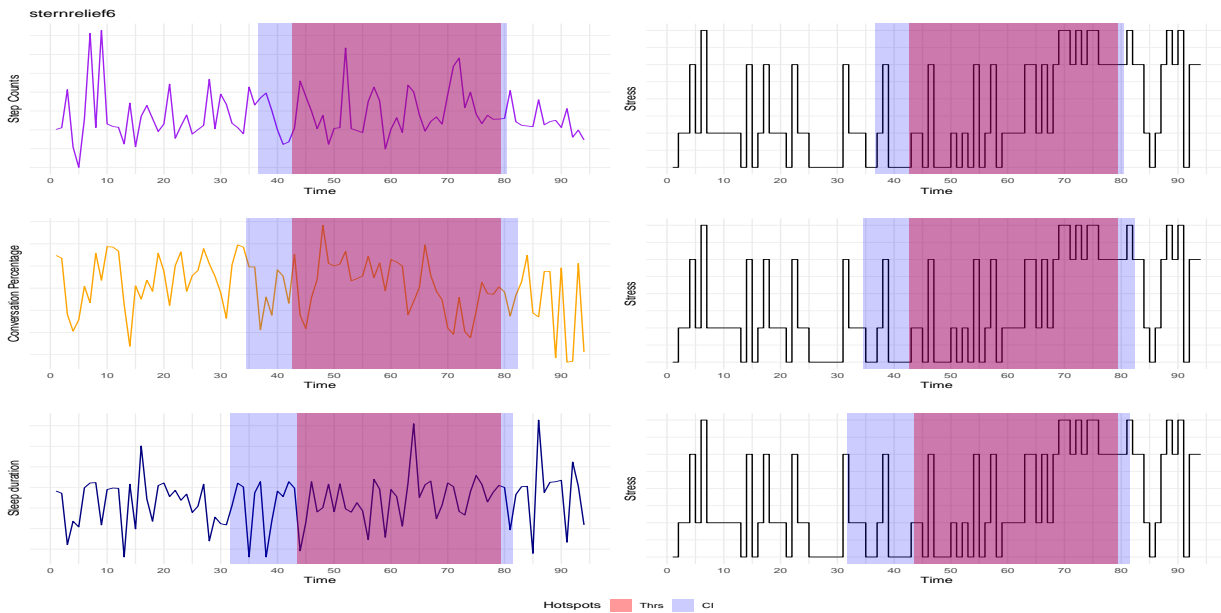


Figure 7: Results of the identified hotspots for sternrelief6 with  $G = 40$  across three combinations of passive sensing variables (left; step count, conversation percentage, and sleep duration in each row) and stress levels (right). The two definitions, threshold and confidence interval rules, are shown as red and blue shaded areas, respectively.

## References

- Abolhassani, A. and Prates, M. O. (2021). An up-to-date review of scan statistics. *Statistic Surveys*, 15:111–153.
- Aminikhanghahi, S. and Cook, D. J. (2017). A survey of methods for time series change point detection. *Knowledge and Information Systems*, 51(2):339–367.
- Baretta, D., Koch, S., Buekers, J., Garcia-Aymerich, J., Knapova, L., Elavsky, S., Godino, J., Olthof, M., Lichtwarck-Aschoff, A., den Hartigh, R., et al. (2025). Predicting recovery after stressors using step count data derived from activity monitors. *npj Digital Medicine*, 8(1):606.
- Bauer, P. and Hackl, P. (1980). An extension of the MOSUM technique for quality control. *Technometrics*, 22(1):1–7.
- Belitser, E. and Ghosal, S. (2025). Bayesian uncertainty quantification and structure detection for multiple change points models. *Bernoulli*, 31(2):1181–1205.
- Bustamante, C. M. V., Coombs III, G., Rahimi-Eichi, H., Mair, P., Onnela, J.-P., Baker, J. T., and Buckner, R. L. (2024). Precision assessment of real-world associations between stress and sleep duration using actigraphy data collected continuously for an academic year: Individual-level modeling study. *JMIR Formative Research*, 8(1):e53441.
- Cappello, L. and Madrid Padilla, O. H. (2025). Bayesian variance change point detection with credible sets. *IEEE Transactions on Pattern Analysis and Machine Intelligence*, 47(6):4835–4852.
- Chen, H. and Zhang, N. (2015). Graph-based change-point detection. *The Annals of Statistics*, 43(57):139–176.
- Cho, H. (2016). Change-point detection in panel data via double CUSUM statistic. *Electronic Journal of Statistics*, 10:2000–2038.
- Cho, H. and Fryzlewicz, P. (2015). Multiple-change-point detection for high dimensional time series via sparsified binary segmentation. *Journal of the Royal Statistical Society Series B: Statistical Methodology*, 77(2):475–507.
- Cho, H. and Kirch, C. (2022). Bootstrap confidence intervals for multiple change points based on moving sum procedures. *Computational Statistics & Data Analysis*, 175:107552.
- Cho, H. and Kirch, C. (2024). Data segmentation algorithms: univariate mean change and beyond. *Econometrics and Statistics*, 30:76–95.
- Chu, C.-S. J., Hornik, K., and Kaun, C.-M. (1995). MOSUM tests for parameter constancy. *Biometrika*, 82(3):603–617.
- daSilva, A. W., Huckins, J. F., Wang, W., Wang, R., Campbell, A. T., and Meyer, M. L. (2021). Daily perceived stress predicts less next day social interaction: Evidence from a naturalistic mobile sensing study. *Emotion*, 21(8):1760.
- Del Angel, M., Nunes, M., Peacock, O., Cranwell, E., and Thompson, D. (2025). Analysing longitudinal wearable physical activity data using non-stationary time series models. *International Journal of Behavioral Nutrition and Physical Activity*, 22(1):88.
- Doraiswamy, P., Khan, Z., Donahue, R., and Richard, N. (2002). The spectrum of quality-of-life impairments in recurrent geriatric depression. *The Journals of Gerontology Series A: Biological Sciences and Medical Sciences*, 57(2):M134–M137.

- Dunn, P. K. and Smyth, G. K. (1996). Randomized quantile residuals. *Journal of Computational and Graphical Statistics*, 5(3):236–244.
- Eichinger, B. and Kirch, C. (2018). A MOSUM procedure for the estimation of multiple random change points. *Bernoulli*, 24(1):526–564.
- Frick, K., Munk, A., and Sieling, H. (2014). Multiscale change point inference. *Journal of the Royal Statistical Society Series B: Statistical Methodology*, 76(3):495–580.
- Fryzlewicz, P. (2014). Wild binary segmentation for multiple change-point detection. *The Annals of Statistics*, 42(6):2243–2281.
- Gomes, N., Pato, M., Lourenco, A. R., and Datia, N. (2023). A survey on wearable sensors for mental health monitoring. *Sensors*, 23(3):1330.
- Hosseini, S., Gottumukkala, R., Katragadda, S., Bhupatiraju, R. T., Ashkar, Z., Borst, C. W., and Cochran, K. (2022). A multimodal sensor dataset for continuous stress detection of nurses in a hospital. *Scientific Data*, 9(1):255.
- Hušková, M. (1990). Asymptotics for robust MOSUM. *Commentationes Mathematicae Universitatis Carolinae*, 31(2):345–356.
- Hyun, S., G’Sell, M., and Tibshirani, R. J. (2016). Exact post-selection inference for changepoint detection and other generalized lasso problems. *arXiv preprint arXiv:1606.03552*.
- Jackson, B., Scargle, J. D., Barnes, D., Arabhi, S., Alt, A., Gioumoussis, P., Gwin, E., Sangtrakulcharoen, P., Tan, L., and Tsai, T. T. (2005). An algorithm for optimal partitioning of data on an interval. *IEEE Signal Processing Letters*, 12(2):105–108.
- James, N. A. and Matteson, D. S. (2015). ecp: An R package for nonparametric multiple change point analysis of multivariate data. *Journal of Statistical Software*, 62:1–25.
- Killick, R. and Eckley, I. A. (2014). changepoint: An R package for changepoint analysis. *Journal of Statistical Software*, 58:1–19.
- Killick, R., Fearnhead, P., and Eckley, I. A. (2012). Optimal detection of changepoints with a linear computational cost. *Journal of the American Statistical Association*, 107(500):1590–1598.
- Kim, Y., Basu, S., and Banerjee, S. (2025). A co-segmentation algorithm to predict emotional stress from passively sensed mhealth data. *Statistics in Medicine*, 44(10-12):e70099.
- Kyriakou, K., Resch, B., Sagl, G., Petutschnig, A., Werner, C., Niederseer, D., Liedlgruber, M., Wilhelm, F., Osborne, T., and Pykett, J. (2019). Detecting moments of stress from measurements of wearable physiological sensors. *Sensors*, 19(17):3805.
- Lee, J., Solomonov, N., Banerjee, S., Alexopoulos, G. S., and Sirey, J. A. (2021). Use of passive sensing in psychotherapy studies in late life: A pilot example, opportunities and challenges. *Frontiers in Psychiatry*, 12:732773.
- Levajković, T. and Messer, M. (2023). Multiscale change point detection via gradual bandwidth adjustment in moving sum processes. *Electronic Journal of Statistics*, 17(1):70–101.
- Li, H., Munk, A., and Sieling, H. (2016). FDR-control in multiscale change-point segmentation. *Electronic Journal of Statistics*, 10:918–959.
- Maharjan, S. M., Poudyal, A., van Heerden, A., Byanjankar, P., Thapa, A., Islam, C., Kohrt, B. A., and Hagaman, A. (2021). Passive sensing on mobile devices to improve mental health services with adolescent and young mothers in low-resource settings: the role of families in feasibility and acceptability. *BMC Medical Informatics and decision making*, 21(1):117.

- Matteson, D. S. and James, N. A. (2014). A nonparametric approach for multiple change point analysis of multivariate data. *Journal of the American Statistical Association*, 109(505):334–345.
- Meier, A., Kirch, C., and Cho, H. (2021). mosum: A package for moving sums in change-point analysis. *Journal of Statistical Software*, 97:1–42.
- Messer, M. (2022). Bivariate change point detection: joint detection of changes in expectation and variance. *Scandinavian Journal of Statistics*, 49(2):886–916.
- Messer, M., Albert, S., and Schneider, G. (2018). The multiple filter test for change point detection in time series. *Metrika*, 81(6):589–607.
- Mohr, D. C., Zhang, M., and Schueller, S. M. (2017). Personal sensing: understanding mental health using ubiquitous sensors and machine learning. *Annual review of clinical psychology*, 13(1):23–47.
- Moser, M. K., Resch, B., and Ehrhart, M. (2023). An individual-oriented algorithm for stress detection in wearable sensor measurements. *IEEE Sensors Journal*, 23(19):22845–22856.
- Murphy, R. A., Hagaman, A. K., Reinders, I., Steeves, J. A., Newman, A. B., Rubin, S. M., Satterfield, S., Kritchevsky, S. B., Yaffe, K., Ayonayon, H. N., et al. (2016). Depressive trajectories and risk of disability and mortality in older adults: longitudinal findings from the health, aging, and body composition study. *Journals of Gerontology Series A: Biomedical Sciences and Medical Sciences*, 71(2):228–235.
- Padilla, O. H. M., Yu, Y., Wang, D., and Rinaldo, A. (2021). Optimal nonparametric multivariate change point detection and localization. *IEEE Transactions on Information Theory*, 68(3):1922–1944.
- Pein, F., Sieling, H., and Munk, A. (2017). Heterogeneous change point inference. *Journal of the Royal Statistical Society Series B: Statistical Methodology*, 79(4):1207–1227.
- Sano, A., Taylor, S., McHill, A. W., Phillips, A. J., Barger, L. K., Klerman, E., and Picard, R. (2018). Identifying objective physiological markers and modifiable behaviors for self-reported stress and mental health status using wearable sensors and mobile phones: observational study. *Journal of Medical Internet Research*, 20(6):e210.
- Saylam, B. and İncel, Ö. D. (2023). Quantifying digital biomarkers for well-being: stress, anxiety, positive and negative affect via wearable devices and their time-based predictions. *Sensors*, 23(21):8987.
- Sheikh, M., Qassem, M., and Kyriacou, P. A. (2021). Wearable, environmental, and smartphone-based passive sensing for mental health monitoring. *Frontiers in Digital Health*, 3:662811.
- Solomonov, N., Kerchner, D., Bein, O., Lee, C. E., Diaz, J. L., Ciarleglio, A., Kim, S., Sirey, J. A., Gunning, F. M., Raue, P. J., et al. (2025). Precision assignment to psychosocial interventions for late-life depression: An automated treatment decision rule. *JAMA Psychiatry*.
- Triantafyllou, S., Saeb, S., Lattie, E. G., Mohr, D. C., and Kording, K. P. (2019). Relationship between sleep quality and mood: ecological momentary assessment study. *JMIR Mental Health*, 6(3):e12613.
- Truong, C., Oudre, L., and Vayatis, N. (2018). ruptures: change point detection in Python. *arXiv preprint arXiv:1801.00826*.
- Truong, C., Oudre, L., and Vayatis, N. (2020). Selective review of offline change point detection methods. *Signal Processing*, 167:107299.
- Vos, G., Trinh, K., Sarnyai, Z., and Azghadi, M. R. (2023). Generalizable machine learning for stress monitoring from wearable devices: A systematic literature review. *International Journal of Medical Informatics*, 173:105026.
- Vostrikova, L. Y. (1981). Detecting “disorder” in multidimensional random processes. *Doklady Akademii Nauk*, 259(2):270–274.

Zhang, H., Diaz, J. L., Kim, S., Yu, Z., Wu, Y., Carter, E., and Banerjee, S. (2024). 2SpamH: a two-stage pre-processing algorithm for passively sensed mHealth data. *Sensors (Basel, Switzerland)*, 24(21):7053.